

Multi-phase-field simulation of austenite-to-ferrite transformation in Fe-C-Mn and Fe-C-Mn-Si alloys

Akinori Yamanaka^{1*}, Masahito Segawa², Takahiko Kohtake³, Raika Yada⁴ and Sukeharu Nomoto²

¹ Division of Advanced Mechanical Systems Engineering, Institute of Engineering, Tokyo University of Agriculture and Technology, 2-24-16, Naka-cho, Koganei-shi, Tokyo, 184-8588, Japan

² Science & Engineering Systems Division, ITOCHU Techno-Solutions Corporation (CTC), Kasumigaseki Bldg., 3-2-5, Kasumigaseki, Tokyo, 100-6080, Japan

³ Nippon Steel & Sumitomo Metal Corporation, 1-8, Fuso-cho, Amagasaki, Hyogo, 660-0891, Japan

⁴ Department of Mechanical Systems Engineering, Faculty of Engineering, Tokyo University of Agriculture and Technology, 2-24-16, Naka-cho, Koganei-shi, Tokyo, 184-8588, Japan

Abstract: This study investigates the austenite-to-ferrite ($\gamma \rightarrow \alpha$) and ferrite-to-austenite ($\alpha \rightarrow \gamma$) transformation behaviours during cyclic heating and cooling processes in Fe-C-Mn and Fe-C-Mn-Si alloys by the non-equilibrium multi-phase-field (NEMPF) model coupled with CALPHAD-based thermodynamic database. In this paper, we present the effect of the interfacial permeability of solute atoms, which is a model parameter governing the partitioning rate of solute atoms at the α/γ interface, on the cyclic transformation behaviour in a Fe-C-Mn-Si alloy. The simulation results showed that the NEMPF model captured the stagnant stage where the migration of the α/γ interface was pinned in the cooling process, and that the stagnant stage corresponded to the time for switching the polarity of Mn and Si spikes formed at the α/γ interface. The simulation results of the cyclic transformation behaviour in multiple heating-cooling processes showed that when the interfacial permeability of Mn atom was decreased, the length of the stagnant stage significantly extended as the number of cycles increased.

1. INTRODUCTION

Prediction of the austenite-to-ferrite ($\gamma \rightarrow \alpha$) transformation is important for developing advanced high strength steels. Various numerical simulation methodologies have been used for predicting the $\gamma \rightarrow \alpha$ transformation behaviour which strongly depends on temperature and chemical composition of steels. Recently, the phase-field and the multi-phase-field methods have been widely used for simulating microstructure evolutions during the $\gamma \rightarrow \alpha$ transformation in Fe-C binary [1, 2] and Fe-C-Mn ternary alloys [3, 4]. The authors have also investigated the $\gamma \rightarrow \alpha$ transformation behaviour in Fe-C-Mn ternary alloys using the multi-phase-field model coupled with CALPHAD-based thermodynamic database [5]. In this study, we have investigated the cyclic $\gamma \rightarrow \alpha$ and $\alpha \rightarrow \gamma$ transformations in Fe-C-Mn and Fe-C-Mn-Si alloys using the non-equilibrium multi-phase-field (NEMPF) model [6]. We have demonstrated that the model can capture the stagnant stage during the cyclic transformation [7, 8] in the multi-component alloys that include substitutional alloying elements. This paper presents the simulation results of the cyclic transformation in a Fe-C-Mn-Si alloy obtained by the NEMPF model. In particular, we show the effect of the interface permeability parameter that governs the partitioning rate of solute elements on the cyclic transformation behaviour: the migration of α/γ interface and the diffusion of solute elements.

2. NON-EQUILIBRIUM MULTI-PHASE-FIELD MODEL

Consider a system composed of N ferrite and austenite grains and m solute species. In order to simulate the migration of α/γ interface during the phase transformation, the local volume fraction of i^{th} grain is defined using the phase field variables, ϕ_i . The value of ϕ_i is unity inside the i^{th} grain, and varies from 1 to 0 in an interface between the i^{th} and j^{th} grains. On the other hand, the total concentration field variable of the solute atom k ($k = \text{C, Mn, Si}$) is expressed by the mixture-law as:

* Corresponding author. E-mail: a-yamana@cc.tuat.ac.jp, telephone: +81 42 388 7087.

$$c^k = \sum_{i=1}^N \phi_i c_i^k \quad (1)$$

where c_i^k denotes the local concentration field variable of k atom in the i^{th} grain.

Using the phase field and concentration field variables, the total free energy of the system is defined as the sum of the gradient energy, the double-well potential energy and the chemical free energy as [9]:

$$G = \int_V \left[\sum_{i=1}^N \sum_{\substack{j=1 \\ j \neq i}}^N \left(-\frac{a_{ij}^2}{2} \nabla \phi_i \cdot \nabla \phi_j \right) + \sum_{i=1}^N \sum_{\substack{j=1 \\ j \neq i}}^N W_{ij} \phi_i \phi_j + \sum_{i=1}^N \phi_i f_i + \sum_{j=1}^{m-1} \lambda^j \left[c^j - \sum_{i=1}^N (\phi_i c_i^j) \right] \right] dV \quad (2)$$

where f_i is the chemical free energy density of the i grain. In this study, the chemical free energy are obtained from Thermo-Calc software [10]. λ^j is a Lagrange multiplier which is used for satisfying Eq. (1). a_{ij} and W_{ij} are the gradient coefficient and height of the double-well potential between the i^{th} and j^{th} grains, respectively. These parameters are given as functions of the interfacial energy between the i^{th} and j^{th} grains, σ_{ij} , and the thickness of diffuse interface, δ , [6].

The time evolution equation of the local concentration field variable for the NEMPF model is expressed as [6]:

$$\frac{\partial c_i^k}{\partial t} = P_i^k \sum_{j=1}^N \phi_j \left(\frac{\partial f_j}{\partial c_j^k} - \frac{\partial f_i}{\partial c_i^k} \right) - \sum_{j=1}^N \frac{\partial \phi_j}{\partial t} (c_j^k - c_i^k) \quad (3)$$

where P_i^k is called as the interfacial permeability [6, 9] and describes the kinetic coefficient of the diffusion of k atom in the i^{th} grain. Because this parameter governs the partitioning rate of solute elements in the α/γ interface, the diffusion behavior of solute atoms during the phase transformation under various conditions can be simulated by changing the value of P_i^k . It should be noted that Eq. (3) is solved for simulating the solute partitioning only in the α/γ interfacial region, while the evolution of the total concentration field variable is calculated by solving the following diffusion equation:

$$\frac{\partial c^k}{\partial t} = \nabla \cdot \left\{ \sum_{i=1}^N \phi_i \sum_{j=1}^{m-1} D_{kj}^i \nabla c_i^j \right\} \quad (4)$$

where D_{kj}^i is the diffusion coefficient of the solute atom k in the i^{th} grain. In this study, the diffusion coefficients are calculated by the method proposed by Anderson et al. [11] using the diffusion mobility data obtained from Thermo-Calc software.

On the other hand, the time evolution of the phase field variable which describes the migration of an interface is given by the following equation [6, 9, 12]:

$$\frac{\partial \phi_i}{\partial t} = \sum_{j=1}^N \frac{2\tilde{M}_{ij}}{N} \left[\sum_{k=1}^N \left\{ \left(\frac{\pi^2}{\delta^2} \phi_k - \nabla^2 \phi_k \right) (\sigma_{jk} - \sigma_{ik}) \right\} + \frac{2\pi}{\delta} \sqrt{\phi_i \phi_j} \Delta \tilde{g}_{ij} \right] \quad (5)$$

where \tilde{M}_{ij} and $\Delta \tilde{g}_{ij}$ are the phase field mobility and the chemical driving force of the phase transformation:

$$\tilde{M}_{ij} = \frac{\delta N M_{ij}}{2\delta N + M_{ij} 2\pi \sqrt{\phi_i \phi_j} \sum_{k=1}^{n-1} \frac{(c_j^k - c_i^k)^2}{P_i^k}} \quad (6)$$

$$\Delta \tilde{g}_{ij} = f_j - f_i - \sum_{k=1}^{n-1} \left(\sum_{l=1}^N \phi_l \frac{\partial f_l}{\partial c_l^k} \right) (c_j^k - c_i^k) \quad (7)$$

where M_{ij} is the mobility of the interface between the i^{th} and j^{th} grain.

It is important to note that in order to reduce computational cost, we employ the interpolation functions of the thermodynamic data; the chemical free energy density, the chemical potential, and the diffusion mobility in the α and γ phases that are derived from Thermo-Calc software with TCFE7 and MOBFE2 databases. The detail of the interpolation function can be found in the author's paper [6].

3. SIMULATION CONDITION

One-dimensional simulations of the cyclic transformation in the $\alpha + \gamma$ two-phase region for Fe-0.023C-0.17Mn-0.2Si [wt.%] alloy are performed. The length of the computational domain is 20 μm . The α phase with a thickness of 1 μm is located at the origin of the computational domain and the other domain is defined as the γ phase. The initial distribution of the solute atoms are set to be uniform over the whole computational domain. Table 1 shows the physical values and parameters used in this study. It is important to note that the thickness of the diffuse interface is set to be submicrometer in order to simulate the stagnant stage in the cyclic transformation. The mobility of α/γ interface is given by the Arrhenius-type equation:

$$M_{ij} = M_0 \exp\left(-\frac{Q}{RT}\right) \quad (8)$$

In order to investigate the effect of the interfacial permeability on the cyclic transformation behavior, we test two different cases of the interfacial permeability as listed in Table 2. For the case 1, the values of the interfacial permeability used in the previous study [6] are used as a reference. The reference values were set to the highest value with which we could perform a stable computation for a given grid spacing and time increment. For the case 2, the interfacial permeability of Mn atom is set to be lower than that in the reference case (the case 1). For both cases, the value of interfacial permeability of solute atoms in the γ phase is set to be the same as that in the α phase.

The cyclic transformations are simulated for the temperature profile shown in Fig. 1. Firstly, an isothermal holding at 1133 K for 150 s is used to obtain an initial $\alpha + \gamma$ two phase microstructure. Then, the heating and cooling processes between 1133 K and 1158 K are repeated for every 150 s at the rate of 10 K/min.

Table 1. Physical values and parameters used in this study [6].

Interfacial energy, σ_{ij}	0.5 [J/m ²]
Activation energy, Q	1.4×10^5 [J/mol]
Gas constant, R	8.314 [J/(K·mol)]
Pre-exponential factor, M_0	3.5×10^{-7} [m ⁴ /(Js)]
Pressure, P	101325 [Pa]
Spacing of finite difference grids, Δx	10 [nm]
Thickness of interface, δ	70 [nm]
Molar volume, V_m	7.09×10^{-6} [m ³ /mol]
Time increment, Δt	1.0×10^{-7} [s]

Table 2. Interfacial permeability of solute atoms used in this study [6].

Case #	P^C [$\text{m}^3/(\text{Js})$]	P^{Mn} [$\text{m}^3/(\text{Js})$]	P^{Si} [$\text{m}^3/(\text{Js})$]
1	10^{-9}	10^{-7}	10^{-7}
2	10^{-9}	10^{-14}	10^{-7}

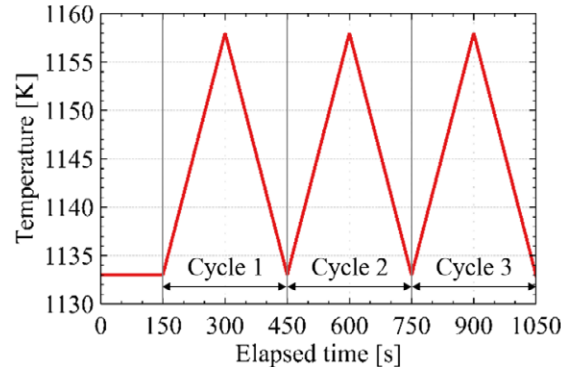


Fig. 1 Temperature profile used for simulating the cyclic $\gamma \rightarrow \alpha$ and $\alpha \rightarrow \gamma$ transformations. The heating and cooling rates are set to be 10 K/min. and -10 K/min., respectively.

4. RESULTS AND DISCUSSION

Fig. 2(a) shows the variations of the α phase volume fraction during the cyclic transformation for three cycles in the case 1. Because the $\alpha \rightarrow \gamma$ transformation occurs in the first heating process, the volume fraction of α phase is reduced continuously. After that, the inverse transformation stage is observed: the reduction of the α phase volume fraction, i.e., the $\alpha \rightarrow \gamma$ transformation, continues, even though the first cooling process starts. Then, we observe the stagnant stage where no phase transformation takes place. It should be noted here that the stagnant stage is defined as the stage where the variation of α volume fraction is less than 0.1%. After the stagnant stage, the $\gamma \rightarrow \alpha$ transformation proceeds in the cooling process. It is seen that the α volume fraction at the end of the first cycle (1133 K and 450 s) is decreased compared to that at the beginning of the first cycle (1133 K and 150 s), which is referred to the transformation hysteresis [6]. The inverse and the stagnant stages are also observed in the second and the third cycles. In the case 1, we find that the length of the stagnant stage does not change even though the number of cycles increases.

On the other hand, as shown in Fig. 2(b), it is found in the case 2 that the length of the stagnant stage in the first cycle is shorter than that in the case 1, while the increase of the number of cycles largely extends the stagnant stage. It is also interestingly shown that the rate of $\gamma \rightarrow \alpha$ transformation after the stagnant stage increases with increasing the cycle number.

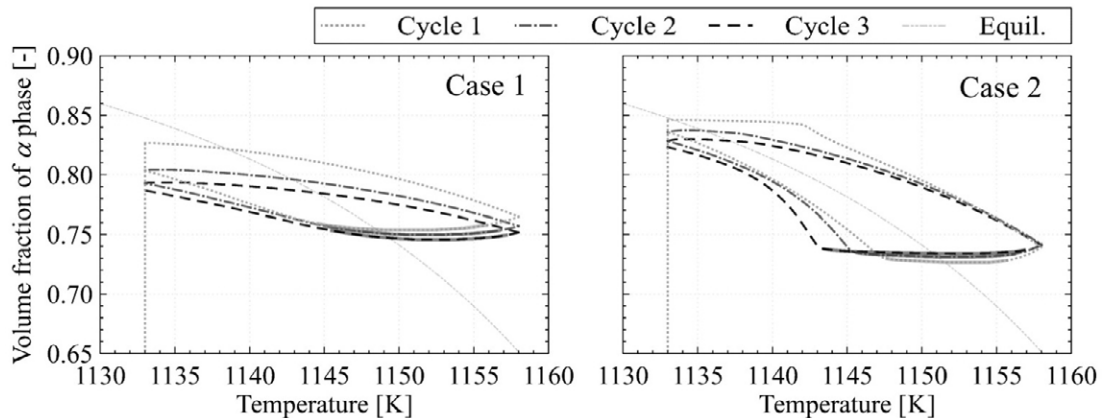


Fig. 2 Variations of α phase volume fraction in the cyclic transformation for different cases. Gray dashed-dotted line indicates the equilibrium volume fraction of α phase calculated by Thermo-Calc software. Gray hatched lines show the stagnant stage where the α volume fraction change is less than 0.1%.

The evolutions of C, Mn and Si concentrations in the first cycle of the cyclic transformation for the case 1 are shown in Fig. 3(a). In the heating process from 1133 K to 1158 K (from 150 s to 300 s), the γ phase grows with the partitioning of interstitial C and substitutional Mn and Si. This γ growth takes place under the local equilibrium (LE)-like mode. In the cooling process from 1158 K to 1133 K (from 300 s to 450 s), the stagnant stage was observed in the early stage of the cooling process as shown in Fig. 2 (a). As already reported in the previous paper [6], in the stagnant stage, the switching of Mn and Si spike polarities occurs and it prevents the migration of the α/γ interface. After the stagnation stage, we observe the growth of α phase which accompanies a positive Mn and a negative Si spikes at the migrating α/γ interface. Thus, this result indicates that the $\gamma \rightarrow \alpha$ transformation after the stagnant stage proceeds under the negligible-partition local-equilibrium (NPLE)-like mode. In the later stage of the cooling process, because the α/γ interface approaches the Mn and Si spikes formed in the initial isothermal holding process, the migration rate of α/γ interface slows down, resulting in the transformation hysteresis.

On the other hand, Fig. 3(b) shows the evolutions of the C, Mn and Si concentrations in the first cycle of the cyclic transformation for the case 2. Although the profiles of C and Si concentrations in the heating and cooling processes are almost the same as those in the case 1, the magnitude of the Mn spike largely decreases as the interfacial permeability of Mn atom decreases, resulting in the shortening of the time for switching the Mn spike polarity, which in turn leads to the shorter stagnant stage in the first cycle than that in the case 1.

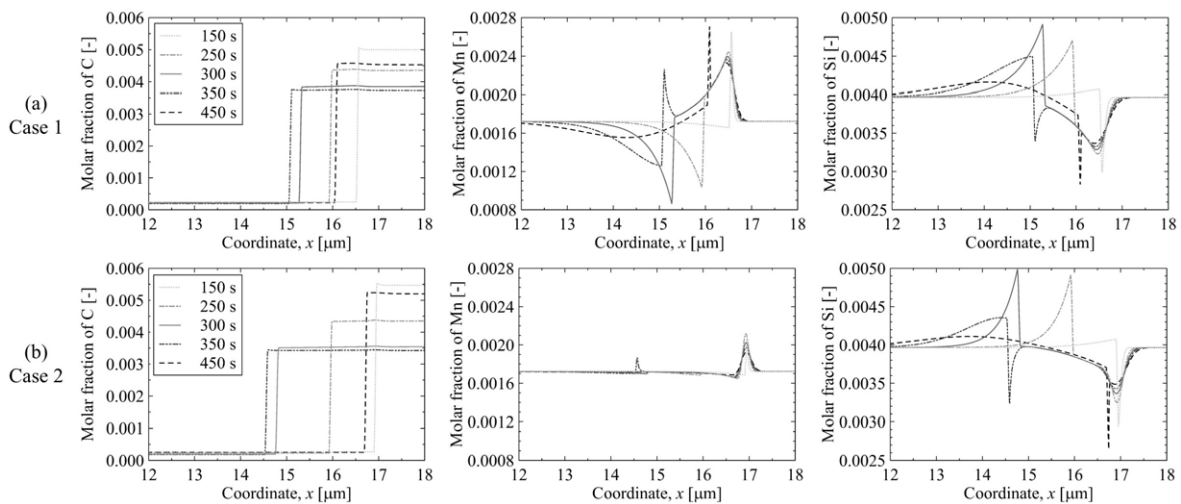


Fig. 3 Evolutions of C, Mn and Si concentrations in the first cycle of the cyclic transformation for (a) the case 1 and (b) the case 2.

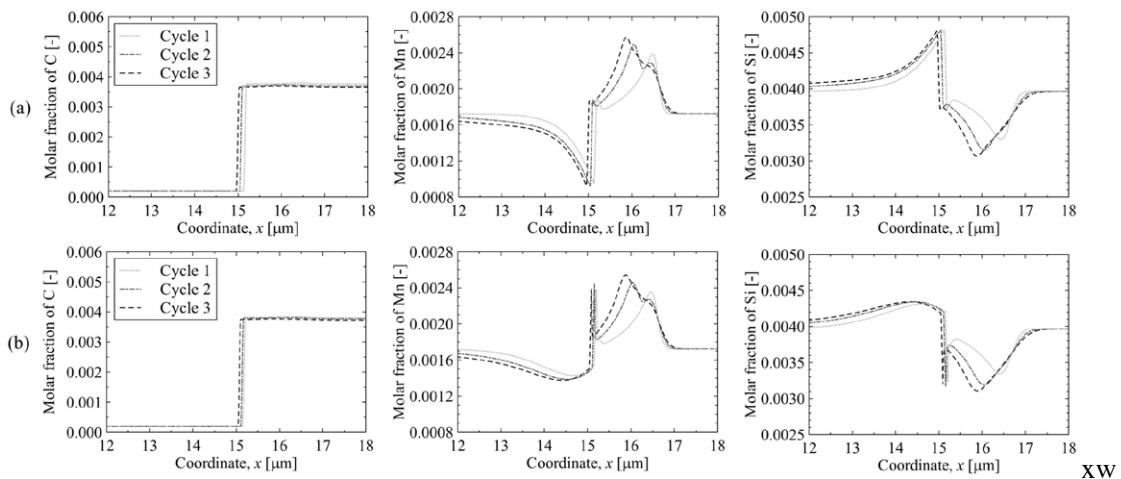


Fig. 4 Profiles of C, Mn and Si concentrations at (a) the beginning and (b) the ending points of the stagnant stage for three cycles in the case 1.

In order to elucidate the variation of the stagnant stage length during the cyclic transformation, Fig. 4 shows the profiles of the C, Mn and Si concentrations at the starting and the ending points of the stagnant stage in three cycles for the case 1. It is seen that the average Mn concentration in the α phase decreases as the cycle number increases, but the minimum Mn concentration in the α phase at the α/γ interface is almost unchanged. On the other hand, the height of Mn spike at the ends of the stagnant stage is almost the same for all cycles. Therefore, the length of stagnant stage would not be changed in the case 1.

Fig. 5 shows the profiles of the C, Mn and Si concentrations at the starting and the ending points of the stagnant stage in the cases 2. It is found from the enlarged Mn profile in Fig. 5(b) that the height of the Mn spike at the ends of the stagnant stage slightly increases as the cycle number increases. Because the permeability of Mn atom in the case 2 is much smaller than that in the case 1, the time for switching the Mn spike polarity significantly increases compared to that in the case 1, resulting in the extension of the stagnant stage in the case 2.

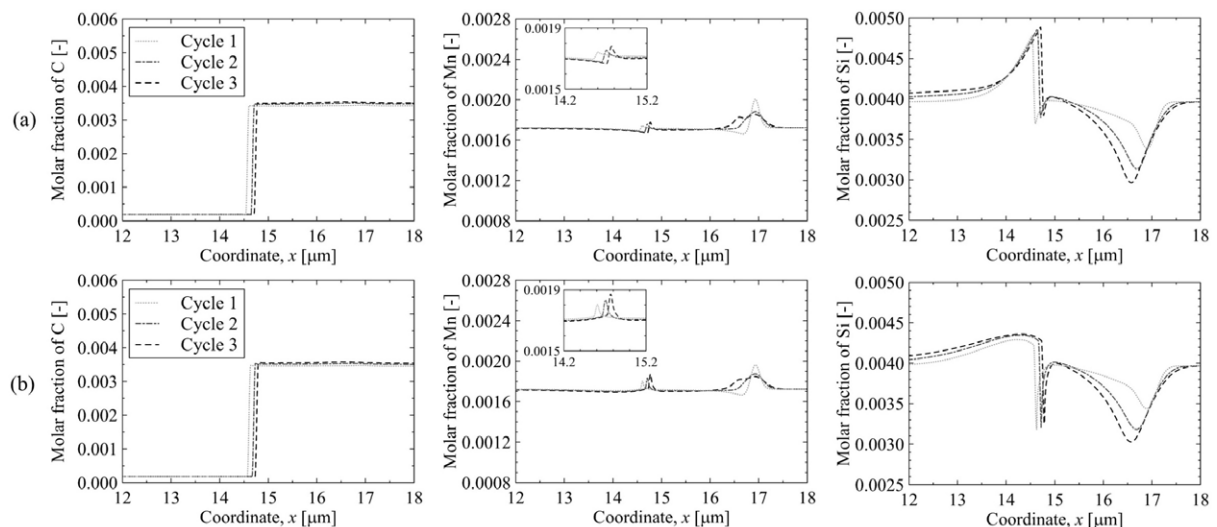


Fig. 5 Profiles of C, Mn and Si concentrations at (a) the beginning and (b) the ending points of the stagnant stage for three cycles in the case 2.

5. CONCLUSION

The cyclic $\gamma \rightarrow \alpha$ and $\alpha \rightarrow \gamma$ transformations in Fe-C-Mn-Si alloy were investigated using the NEMPF model. In particular, the effect of the interfacial permeability of solute atoms on the cyclic transformation behaviour was examined. The simulation results demonstrated that the NEMPF model captured the special features of the cyclic transformation: the inverse transformation stage, the stagnant stage and the transformation hysteresis. We revealed that the decrease of the interfacial permeability of Mn atom extended the time for switching Mn spike polarity, which led to the longer stagnant stage in the later cycles.

REFERENCES

- [1] I. Loginova, J. Odqvist, G. Amberg, J. Ågren: *Acta Materialia*, 51 (2003), 1327-1339.
- [2] A. Yamanaka, T. Takaki, Y. Tomita: *Materials Transaction*, 47 (2006), 2725-2731.
- [3] D-H. Yeon, P-R. Cha, J-K. Yoon: *Scripta Materialia*, 45 (2001), 661-668.
- [4] M. Militzer, M. G. Mecozzi, J. Sietsma, S. van der Zwaag: *Acta Materialia*, 3961-3972.
- [5] T. Kohtake, M. Segawa, A. Yamanaka: *Journal of Crystal Growth*, 468 (2017), 63-67.
- [6] M. Segawa, A. Yamanaka, S. Nomoto: *Computational Materials Science*, 136 (2017), 67-75.
- [7] H. Chen, S. van der Zwaag: *Computational Materials Science*, 49 (2010), 801-813.
- [8] H. Chen, B. Zhu, M. Militzer: *Metallurgical Materials Transactions A*, 47 (2016), 3873-3881.
- [9] I. Steinbach, L. Zhang, M. Plapp: *Acta Materialia*, 60 (2012), 2689-2701.
- [10] <http://www.thermocalc.com> (accessed at 12nd November, 2017)
- [11] J.-O. Anderson, J. Ågren: *Journal of Applied Physics*, 72 (1992), 1350-1355.
- [12] I. Steinbach, F. Pezzolla: *Physica D*, 134 (1999), 385-393.